Microbial influence in Spanish bentonite slurry microcosms: unveiling a-year long geochemical evolution and early-stage copper corrosion related to nuclear waste repositories

Marcos F. Martinez-Moreno[1,*], Cristina Povedano-Priego[1], Mar Morales-Hidalgo[1], Adam D. Mumford[2], Elisabet Aranda[3], Ramiro Vilchez-Vargas[4], Fadwa Jroundi[1], Jesus J. Ojeda[2], and Mohamed L. Merroun[1]

[1]*Faculty of Sciences, Department of Microbiology, University of Granada, Granada, Spain.*

[2]*Department of Chemical Engineering, Faculty of Science and Engineering, Swansea University, Swansea, United Kingdom*

[3]*Institute of Water Research, Department of Microbiology, University of Granada, Granada, Spain*

[4]*Medical Department II, University Hospital, Ludwig-Maximilians-Universität, Munich, Germany*

Keywords

DGR, Spanish bentonite, microbial diversity, electron donors/acceptor, copper corrosion

Abstract

Deep Geological Repository (DGR) concept consist of storing radioactive waste in metal canisters, surrounded by compacted bentonite, and placed into a geological formation. Here, bentonite slurry microcosms with copper canister, inoculated with bacterial consortium and amended with acetate, lactate and sulfate were set up to investigate their geochemical evolution over a year under anoxic conditions. The impact of microbial communities on the corrosion of copper canister in an early-stage (45 days) was also assessed. The amended bacterial consortium and electron donors/acceptor accelerated the microbial activity, while bentonite heat-shocked process had a retarding effect. The microbial communities partially oxidize lactate to acetate which is subsequently consumed when the lactate is depleted. Early-stage microbial communities showed that the bacterial consortium reduced microbial diversity with *Pseudomonas* and *Stenotrophomonas* dominating the community. However, sulfate-reducing bacteria such as *Desulfocurvibacter*, *Anaerosolibacter*, and *Desulfosporosinus* were enriched coupling oxidation of lactate/acetate with reduction of sulfates. The generated biogenic sulfides could mediate the conversion of copper oxides (possibly formed by trapped oxygen molecules on the bentonite or driven by the reduction of H_2O) to copper sulfide (Cu_2S) identified by X-ray photoelectron spectroscopy (XPS). Overall, these findings shed light on the ideal geochemical conditions that would affect the stability of DGR barriers, emphasizing the impact of the SRB on the corrosion of the metal canisters, the gas generation, and the interaction with components of the bentonite.

1_ Introduction

The global challenge of managing high-level radioactive waste (HLW) has led to the consideration of the Deep Geological Repository (DGR) as the internationally accepted option for this propose (WNA, 2023). The main objective is to preserve the long-term integrity and the safety performance of these repositories for periods spanning from several hundreds to millions of years, ensuring that no residual radioactive materials reach the surrounding environment (Betandiieva et al., 2009). The multi-barrier design of DGR consists of a buffering and sealing bentonite-based material surrounding the waste-containing metal canisters that will be placed several hundred meters underground in a stable geological formation to ensure safety until the radiotoxicity diminishes to levels similar to natural ones (Ojovan and Steinmetz, 2022). The nature of the barriers depends on the particular strategy adopted by each country. Copper-coating metal canisters have been proposed, or already implemented, by countries such as Canada, Korea, Sweden, and Finland (Hall et al., 2021). In addition, compacted bentonite clay was selected as the most appropriate buffer and sealing material. This clay provides mechanical support for canisters, prevents groundwater infiltration, retards radionuclides diffusion, and seals canisters in the event of rupture or cracks (García-Romero et al., 2019). In Spain, bentonite from Almeria (FEBEX) has been proposed as buffer material for Spanish DGR (Huertas et al., 2021; Villar et al., 2006).

Since bentonites are not sterile, understanding the structure and composition of the microbial community within this clay could provide insights in its potential impact on the long-term stability and safety of the DGR barriers (Meleshyn et al., 2011). Microorganisms may compromise the mineralogy and chemistry of the bentonite buffer and the integrity of the metal canisters due to microbially influenced corrosion (MIC) via biofilm formation or corrosive metabolite production (Ruiz-Fresneda et al., 2023).

66 Moreover, microbial metabolism may contribute to the production of hydrogen, methane,
67 and carbon dioxide, affecting the gas phase that would increase the pressure within the
68 DGR (Guo & Fall, 2021; Bagnoud et al., 2016).

69 Once the DGR is sealed, the gradual depletion of oxygen will occur due to factors such
70 as microbial activity and metal canister corrosion, leading to the establishment of an
71 anoxic environment (Payer et al., 2019; Keech et al., 2014). In this context, certain
72 anaerobic bacteria such as sulfate-reducing bacteria (SRB) and iron-reducing bacteria
73 (IRB) could remain metabolically active. These bacteria may have adverse consequences,
74 including the promotion of MIC, the reduction of Fe(III) to Fe(II) in smectite (the major
75 mineral in bentonites), and the reduction of sulfate to sulfide (a key agent in copper
76 corrosion) (Pentráková et al., 2013; Liu et al., 2012; Shelobolina et al., 2003). Sulfide
77 production, attributed to SRB activity, is more likely to occur further away from the
78 canisters under conditions that favor SRB growth, such as lower temperatures and higher
79 water activity (Bengtsson and Pedersen, 2017). This biogenic sulfide could diffuse
80 through the biologically inactive section of the sealing materials and influence the nature
81 and rate of canister-surface corrosion.

82 Although the bentonite will be in the form of compacted blocks within the DGR, which
83 is expected to suppress microbial activity, it is necessary to consider all possible scenarios.
84 Therefore, to understand the impact of the microbial activity, including the indigenous
85 microorganisms, on Spanish bentonite over the short term, optimal conditions for
86 microbial growth, representing a worst-case scenario for a DGR, were simulated. In this
87 study, bentonite slurry anaerobic microcosms were amended with acetate, lactate, and
88 sulfate (electron donors and acceptor, respectively) to stimulate microbial activity. Hence,
89 this study aims to comprehensively examine the impact of microorganisms on the
90 geochemical evolution of a complex bentonite slurry systems for one year of anaerobic

incubation. Additionally, the microbial communities and their influence on copper corrosion in an early state (45 days) of incubation within the microcosms were investigated.

Our results emphasize the role of the microorganisms present in the bentonite, which could provide optimal growth conditions in the event of an influx of nutrients due to the filtration of water in the bentonite.

2_ Materials and methods

2.1_ Bentonite sampling

The bentonite was aseptically collected from El Cortijo de Archidona site in Almeria (Spain) in February 2020 (maximum depth: ~ 80 cm). Subsequently, the bentonite was aseptically disaggregated, dried and ground to achieve a uniform powder following the procedure by Martinez-Moreno et al. (2023). The chemical composition of the initial bentonite is specified in the **Supplementary Table S1**.

2.2_ Microcosms assembly and sampling

Procedures related to copper material and mini-canister (Cu-mCan) assembly, elaboration of the different solutions, and BPAS consortium information and culture conditions are detailed in **Supplementary Material**.

Microcosms were set up following the procedure described by Povedano-Priego et al. (2023) with some modifications. Fifty g of ground bentonite was added to 250 mL borosilicate glass bottles previously autoclaved. Solutions of acetate, lactate and sulfate (section 1.1 of **Supplementary Material**) were supplemented in the electron donors/acceptor-containing (eD) microcosms with a final concentration of 30 mM, 10

mM, and 20 mM, respectively. Additionally, the bacterial consortium-containing (BC) bottles were spiked with a BPAS consortium (section 1.2 of **Supplementary Material**) with an initial OD_{600} of 0.4 for each bacterial strain (*Bacillus* sp. BII-C3, *Pseudomonas putida*, *Amycolatopsis ruanii*, and *Stenotrophomonas bentonitica*). The final volume of the microcosms was calculated considering the solutions added and then filled up to 230 mL with the Equilibrium Water (EW) (section 1.1 of **Supplementary Material**). Finally, for corrosion studies, three sterilized high-purity oxygen-free Cu-mCan (section 1.3 of **Supplementary Material**) were deposited into each microcosm.

Different treatments were considered to study the impact of three parameters (sample code between brackets): i) bentonite and heat-shocked bentonite (B and StB), ii) acetate:lactate:sulfate addition (eD), and iii) the addition of a bacterial consortium (BC). Although tyndallization (heat-shock) is not the optimal method for sterilizing bentonite (Martinez-Moreno et al., 2024), StB bentonites were tyndallized (110 ºC for 45 min, 3 consecutive days) to reduce the presence and activity of autochthonous bacteria. A total of 24 microcosms were elaborated (8 treatments in triplicate). The sample ID and characteristic of the treatments are summarized in **Table 1**.

Table 1.
Experimental conditions and sample ID of the different treatments. All free-oxygen microcosms incorporated three Cu mini-canisters (Cu-mCan) and elaborated in triplicate. A:L:S: acetate, lactate, and sulfate concentrations; BPAS: bacterial consortium; +: presence; -: absence.

Sample ID	Bentonite	A:L:S (mM)	BPAS
B.eD.BC	Non-heat-shocked	30:10:20	+
B.BC		-	+
B.eD		30:10:20	-
B		-	-
StB.eD.BC	Heat-shocked	30:10:20	+
StB.BC		-	+
StB.eD		30:10:20	-
StB		-	-

Glossary: B: bentonite, StB: heat-shocked bentonite, eD: addition of electron donors and sulfate, BC: spiked with bacterial consortium

Once the microcosms were completed, the borosilicate bottles were sealed with butyl-rubber stoppers and degassed with N_2 to create anaerobic conditions. Subsequently, microcosms were incubated at 28 ºC for one year. The workflow of the microcosms set-up is shown in **Figure 1**. Samples from the different components (supernatant, bentonite slurry, and Cu-mCan) were recovered aseptically within a glovebox for the different analyses.

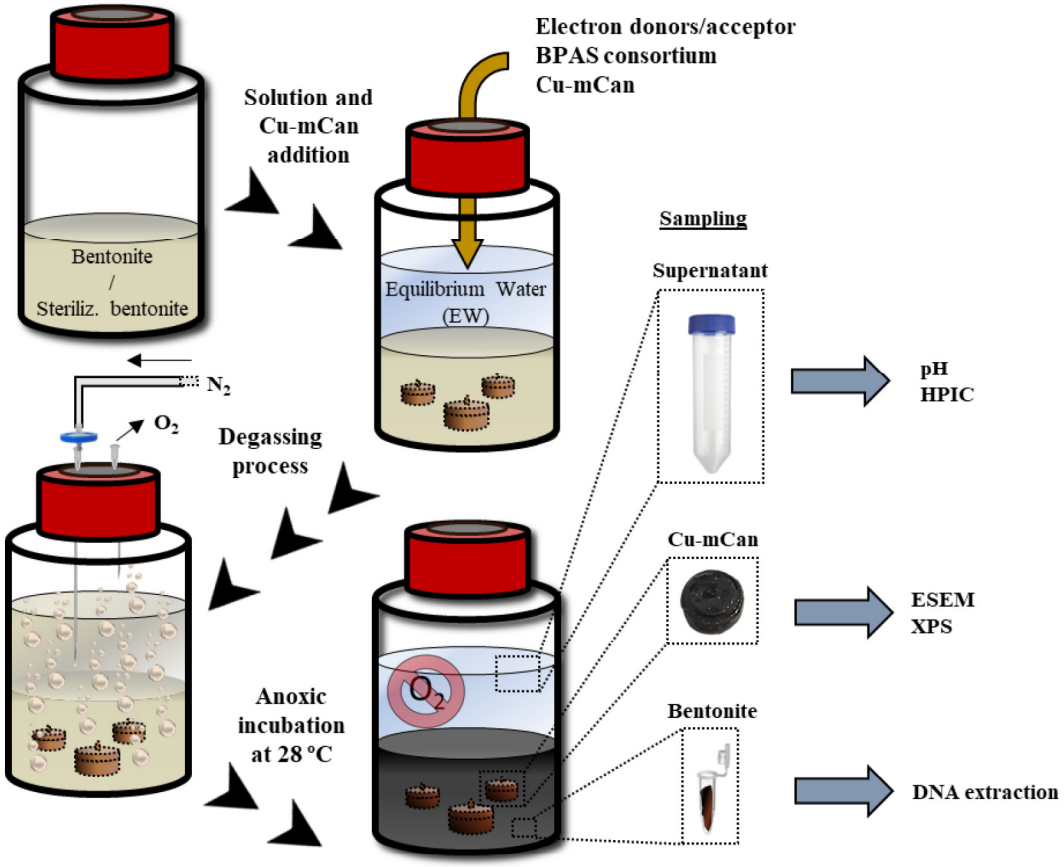

Figure 1. Microcosms workflow, N_2 degassing process (anaerobic conditions), and sampling for the different analyses.

2.3_ Geochemical analyses of the microcosm supernatants

For the evolution of geochemical analysis, supernatant (liquid phase) from each microcosm were collected at 45, 90, 135, and 365 days of incubation under anaerobic

146 conditions, and filtered with 0.22 µm cellulose-acetate filter. The pH was measured by
147 Advanced Digital Handheld Portable Meter HQ40D (Hach) previously calibrated with
148 commercial reference solutions (4.00 and 7.00).

149 Acetate, lactate, and sulfate concentrations in the supernatants from the amended samples
150 (eD) were quantified by High Pressure Ion Chromatography (HPIC) to understand the
151 chemical evolution of these added compounds. The analysis was performed in a 925 Eco
152 ICE, Methrom Hispania (Herisau, Switzerland) coupled with an IC conductivity detector,
153 a Metrohm Suppressor Module (MSM), 250 µL injection loop with peristaltic pump,
154 Metrohm high pressure pump with purge valve and 919 UF autosampler. Before injection,
155 samples were 0.22 µm filter-sterilized and diluted in ultrapure water. Measurement
156 specifications are detailed in section 1.4 of the **Supplementary Material**.

157 **2.4_ DNA extraction, sequencing, and computational procedure**

158 DNA extraction was performed for each microcosm at 45 days incubation following the
159 procedure detailed in Povedano-Priego et al. (2021) in order to characterize the microbial
160 community within the microcosms in an early-stage incubation and their implication on
161 the alteration of the Cu-mCans. Subsequent, the extracted DNA concentration was
162 determined using Qubit 3.0 Fluorometer (Life Technology, Invitrogen™).

163 For the library preparation, two consecutive PCR reactions were carried out for each
164 sample using a combination of regular and barcoded fusion primers to amplify the V5 -
165 V6 variable regions of the 16S rRNA gene (see details in section 1.5 of **Supplementary**
166 **Material**). Libraries were sequenced using the MiSeq Illumina platform (2 × 250 bp,
167 Hayward, California, USA).

FastaQ files were processed and normalized employing “dada2” and “phyloseq” packages, respectively, in R 4.2.1 software (R Core Team, 2022). Bayesian classification was employed to assign the phylotypes to a taxonomic affiliation (80% pseudo-bootstrap threshold). The relative abundances and alpha diversity indices were conducted using Explicet 2.10.5 (Robertson et al., 2013). To assess the similarity between samples at genus level, a matrix based on the Bray-Curtis algorithm was used, and subsequent similarity between samples was performed through Principal Coordinate Analysis (PCoA) using Past4 software (Hammer et al., 2001). Furthermore, a heatmap was performed to visualize taxa with more than 0.50% relative abundance. For this purpose, the 'heatmap.2' function was employed in R software.

2.5_ Surface characterization of the copper mini canisters (Cu-mCan)

After 45 days of anoxic incubation, the Cu-mCan were removed from the microcosms, unscrewed, and dried under anaerobic atmosphere. To visualize corrosion compounds on the surface, the base of the Cu-mCan was metallized with a carbon coating through evaporation by an EMITECH K975X Carbon Evaporator for analysis by High Resolution Scanning Electron Microscopy (HRSEM) with an AURIGA Carl Zeiss SMT microscope associated with a qualitative and quantitative energy dispersive X-ray energy dispersive (EDX) microanalysis.

Moreover, no previous preparation was applied to the lids of the Cu-mCan for spectroscopic analysis. The chemical analysis by X-ray photoelectron spectroscopy (XPS) of the lid’s surface was conducted on a Kratos AXIS Supra Photoelectron Spectrometer. Spectra acquisition and detailed information is shown in section 1.6 of the **Supplementary Material**. Finally, CasaXPS 2.3.22 software (Fairley, 2019) was used to

191 fit the peaks of the XPS spectra. All binding energies were offset by referencing the
192 adventitious carbon C1s peak (285 eV).

193 **3_ Results and discussion**

194 **3.1_ Water chemistry evolution**

195 Untreated bentonite is expected to have an initially alkaline pH around 9.00 due to its
196 innate buffering capacity (Povedano-Priego et al., 2019; Rozalén et al., 2009). After one-
197 year incubation, pH values tended to stabilize between 7.51 and 8.37 in all treatments, in
198 contrast to the initial values (**Supplementary Figure S2**). The observed pH decrease
199 could be due to leaching of the bentonite or microbial activity through the generation of
200 gases such as hydrogen (H_2), methane (CH_4), and carbon dioxide (CO_2) (Fernández-Díaz
201 2004; Povedano-Priego et al., 2019; Bagnoud et al., 2016).

202 Lactate was the first electron donor to be consumed (**Figure 2A**). Complete depletion was
203 achieved at 45 days in the microcosms spiked with the bacterial consortium (B.eD.BC)
204 in contrast to its heat-shocked counterpart StB.eD.BC where lactate was consumed after
205 45 days. In microcosms without the bacterial consortium lactate was slowly consumed
206 reaching complete depletion at 135 days (B.eD) and 365 days (StB.eD). Regarding acetate
207 evolution (**Figure 2B**), in the sample B.eD.BC acetate was gradually depleted following
208 the consumption of lactate being nearly exhausted after one year-incubation. In the other
209 treatments, acetate initially increased before being consumed, with complete depletion
210 occurring around one year-incubation in B.eD. This could suggest that acetate is produced
211 from lactate consumption and subsequently used as an electron donor. Sulfate
212 consumption (**Figure 2C**) was highest in the non-heat-shocked samples containing the
213 bacterial consortium (≈50% in B.eD.BC). In the samples B.eD, StB.eD.BC, and StB.eD,

214 sulfate levels remained relatively stable for most of the incubation period, only decreasing
215 to about 20-30% after one year.

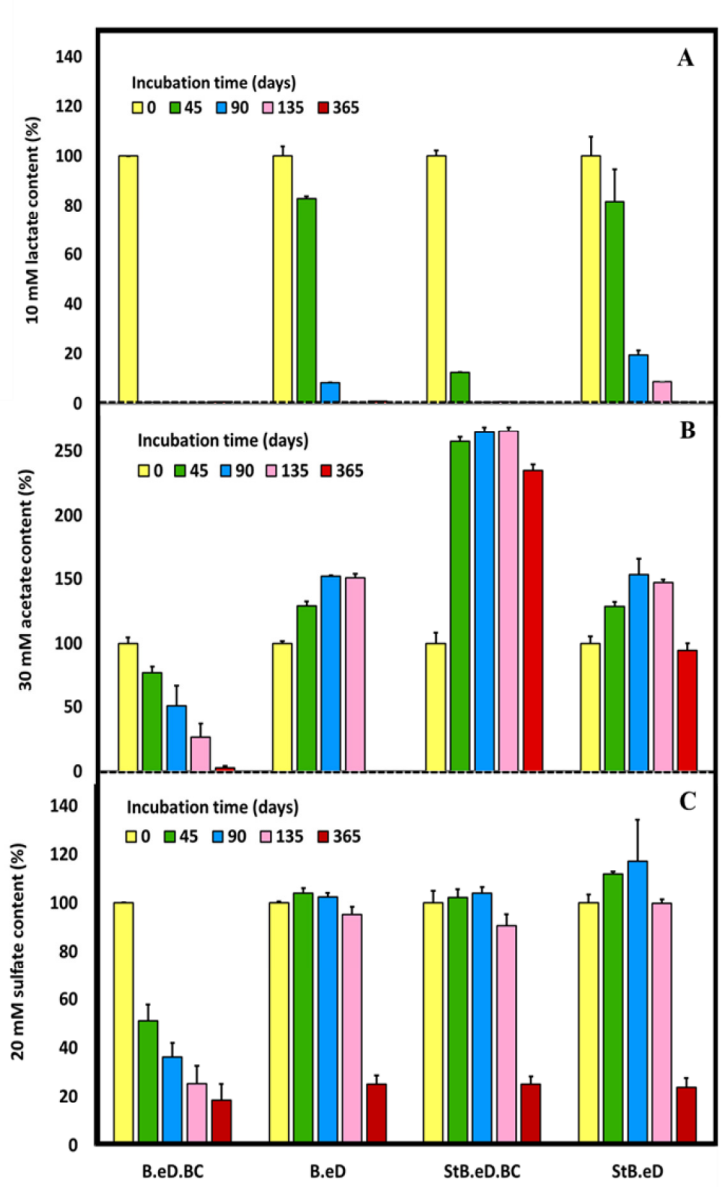

Figure 2. Evolution of the initial concentration of 10 mM lactate (A), 30 mM acetate (B), and 20 mM sulfate (C) content recorded in Spanish bentonite microcosms incubated anaerobically at 30 ºC for 1 year. Data showed the mean values with standard derivations measured from three independent replicates. Glossary: B: bentonite, StB: heat-shocked bentonite, eD: addition of electron donors and sulfate, BC: spiked with bacterial consortium.

216 In general terms, the tyndallization of the bentonite (heat-shocked samples) seems to slow
217 down the dynamics of lactate and acetate, and sulfate reduction when compared with the
218 non-heat-shocked samples. This indicates that tyndallization adversely affects microbial

219 activity. Moreover, the bacterial consortium seems to enhance lactate consumption and
220 acetate production/consumption.

221 The conversion of lactate to acetate, in the absence of sulfate reduction, could occur via
222 lactate fermentation to acetate and propionate, or its incomplete oxidation to acetate
223 coupled with iron reduction (Park et al., 2024). The consumption of sulfate in the sample
224 B.eD.BC is supported by the work of Matschiavelli et al. (2019) as they observed a
225 decrease in lactate and sulfate concentrations concomitant with acetate formation in B25
226 Bavarian bentonite microcosms. Their study deduced that through the reductive pathway
227 of acetyl-CoA lactate is incompletely oxidized to acetate with the concurrent reduction of
228 sulfate to hydrogen sulfide. The presence of fissures in the bentonite (white arrows in
229 **Figure 3**) and the formation of small bubbles in the microcosms could be related to gas
230 generated from microbial activity. The rotten egg odor after sampling procedure could
231 support also the hydrogen sulfide (H_2S) formation (He et al., 2011). The visual color
232 changes reported in the bentonite microcosms during the incubation are also observed in
233 **Figure 3**. A shift towards black hues was evidenced in the treatment containing the
234 bacterial consortium (B.eD.BC), with this transformation occurring at a slower rate when
235 the bentonite was heat-shocked (StB.eD.BC). Subsequently, the treatments lacking the
236 bacterial consortium (B.eD, and StB.eD) exhibited similar color changes, although with
237 lower progression. The alteration in the color of the bentonite may be linked to the
238 generation of H_2S, a byproduct of bacterial activity, which can react with iron and lead to
239 the formation of black precipitates of reduced iron species (Miettinen et al., 2022;
240 Matschiavelli et al., 2019).

241

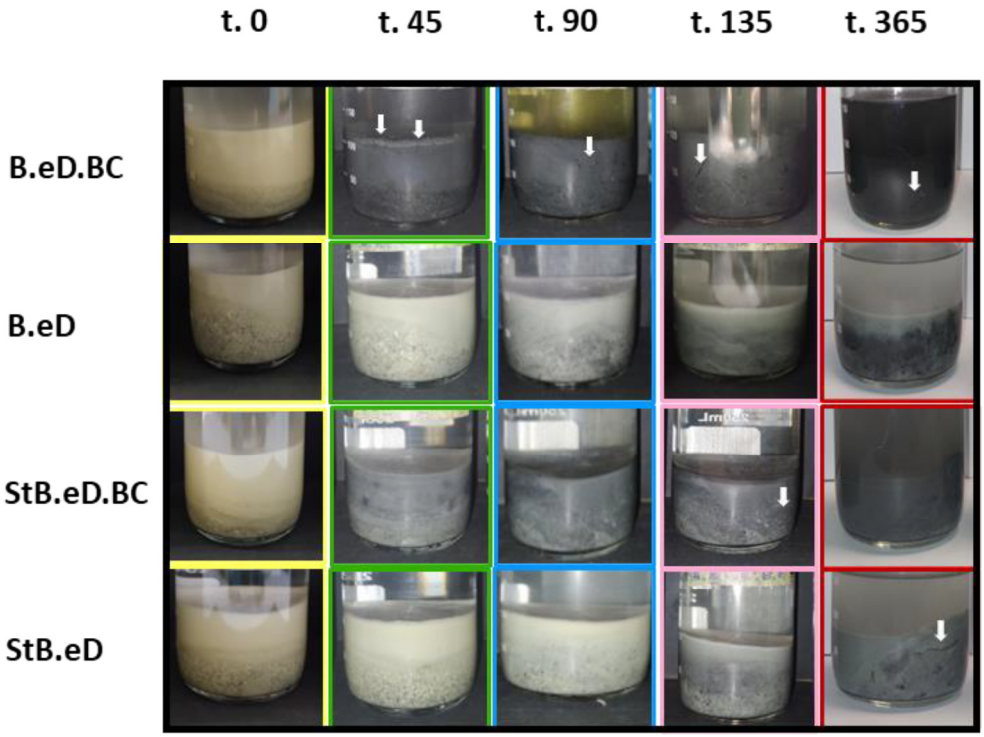

Figure 3. Evolution of hyper-saturated Spanish bentonite microcosms before (yellow) and after 45 (green), 90 (blue), 135 (pink) and 365 (red) days of anaerobic incubation at 30 ºC. White arrows indicate the development of fissures and cavities attributed to gas formation. Glossary: B: bentonite, StB: heat-shocked bentonite, eD: addition of electron donors and sulfate, BC: spiked with bacterial consortium.

242 **3.2_ Characterization of microbial communities in an early incubation stage**

243 The microbial communities of the bentonite microcosms were characterized to get a
244 thorough comprehension of early-stage geochemical changes and their influence on
245 copper corrosion. Thus, the total DNA from the different bentonite microcosms after 45
246 days of anaerobic incubation was extracted and sequenced in triplicate (duplicate in
247 sample StB.eD). The structure and composition of bacterial communities in the different
248 treatments was characterized: tyndallized (StB), presence of electron donors/acceptor
249 (eD), and addition of the bacterial consortium (BC) in the early-stage of incubation (45
250 days) in view of study their early-stage influence in the corrosion of copper material.

For these samples, enough sequencing depth was achieved as shown by the rarefaction curves (**Supplementary Figure S3**). A total of 412 phylotypes were detected and annotated in 13 phyla (98.06%) being Pseudomonadota (74.63%), Bacillota (19.74%), and Actinomycetota (2.67%) the most abundant phyla (**Supplementary Table S4**). At genus level, the phylotypes were annotated in 110 OTUs (**Supplementary Table S5**) with *Pseudomonas* (43.35%), *Stenotrophomonas* (13.41%), unclassified Clostridiales (4.75%), *Pseudoalteromonas* (4.64%), *Symbiobacterium* (4.24%), *Desulfocurvibacter* (3.08%), unclassified Bacillota (2.98%), and *Desulfuromonas* (2.89%) presenting the higher relative abundance in the pool of the samples.

Richness (Sobs), diversity (ShannonH and SimpsonD), and evenness (ShannonE) indices at the genus level of the samples are presented in **Supplementary Table S3**. The richness indices of non-heat-shocked treatments reveal higher values in samples lacking bacterial consortium, and these values are greater in the absence of electron donors and sulfate (richness values B > B.eD > B.eD.BC > B.BC). In contrast, the dynamics in the heat-shocked treatments (StB) seem to be slightly different, with higher richness values in the samples amended with electron donors and sulfate, while the presence of the consortium seemed to affect the richness indices diminishing the effect of electron donors (richness values StB.eD > StB.eD.BC > StB > StB.BC). These results are supported by the diversity indices (ShannonH and SimpsonD) showing the same trends in the samples (**Supplementary Table S3**). The microcosms without bacterial consortium showed greater diversity values (ShannonH > 3, and SimpsonD close to 1) than those spiked with the bacterial consortium (BC), indicating that the addition of this consortium results in a displacement of the indigenous bentonite microbial community and the domination of specific taxa within the samples (ShannonH < 3, and SimpsonD further from 1).

In order to analyze the dissimilarity and diversity distribution along different microcosms considering the relative abundance at genus level, samples were grouped by a Principal Coordinate Analysis (PCoA) based on Bray-Curtis distance (**Figure 4A**). The dissimilarity between samples containing the bacterial consortium and those lacking it was evidenced. The treatments containing bacterial consortium (BC samples) were grouped separately from the other treatments, indicating that the treatments lacking bacterial consortium showed a more heterogeneous distribution.

Moreover, a heatmap was constructed to confirm the similarity between samples (**Figure 4B**). As observed, the clustering of BC samples is primarily attributed to the prevalence of bacterial genera from the BPAS consortium, notably *Pseudomonas* and *Stenotrophomonas*, which dominate the microbial communities of these microcosms. In contrast, for samples lacking a bacterial consortium, a slight differentiation was observed between samples with heat-shocked bentonite (StB) and those with non-heat-shocked bentonite (B) possibly due to the negative effect of the tyndallization process on the microbial diversity of the bentonite (Martinez-Moreno et al., 2023; Povedano-Priego et al., 2023). However, such differentiation was not observed when considering the absence or the presence (eD) of electron donors and sulfate. The main difference between microcosms unamended (B) and amended with electron donors and sulfate (B.eD) resided in the presence of bacterial genera such as *Pseudoalteromonas* (24.17%), *Desulfocurvibacter* (22.72%), *Anaerosolibacter* (4.54%), *Desulfosporosinus* (4.54%), and unclassified microbes belonging to the highly diverse order Bacillales (3.70%) in sample B.eD. Some strains of *Pseudoalteromonas* have adaptive mechanisms to tolerate low oxygen concentrations (Qin et al., 2011) or the ability to use acetate as a carbon source (Oh et al., 2011) which support the distribution of *Pseudoaltermonas* in this treatment. Moreover, the strictly anaerobes *Desulfocurvibacter, Anaerosolibacter* and

300 *Desulfosporosinus* can use sulfate and/or iron as electron acceptor to grow in the presence
301 of organic substrates (e.g., lactate) (Spring et al., 2019; Hong et al., 2015; Hippe and
302 Stackebrandt, 2015).

303 As shown in the heatmap (**Figure 4B**), the dominant genera in the consortium-spiked
304 treatments (BC) were those of the consortium, *Pseudomonas* (54.59%-78.88%) and
305 *Stenotrophomonas* (34.96%-8.10%) (**Supplementary Table S5** and **Figure 5**).
306 *Amycolatopsis*, was detected in lower relative abundance in the BC microcosms
307 exhibiting higher abundance in B.eD.BC and StB.eD.BC samples (2.31% and 2.05%,
308 respectively). In contrast, the presence of *Amycolatopsis* was lower or undetectable in the
309 samples without electron donors and sulfate: 0.12% and 0% (B.BC and StB.BC,
310 respectively). Regarding *Bacillus* genera, was outside the detection range in the samples.
311 *Pseudomonas putida* and *Stenotrophomonas bentonitica* are bacterial strains capable of
312 growing or maintaining their activity under anaerobic conditions, while also exhibiting
313 the ability to use acetate and/or lactate as a carbon source (Freikowski et al., 2010;
314 Sanchez-Castro et al., 2017). *Pseudomonas* was also detected in the microcosms without
315 bacterial consortium with a remarkable relative abundance of 9.80% (B.eD), 19.11% (B),
316 16.48 (StB.eD), and 9.91% (StB). On the other hand, *Stenotrophomonas* was only
317 detected in the heat-shocked treatments (StB.eD and StB) with a 2.66% and 13.98% of
318 relative abundance, respectively.

319

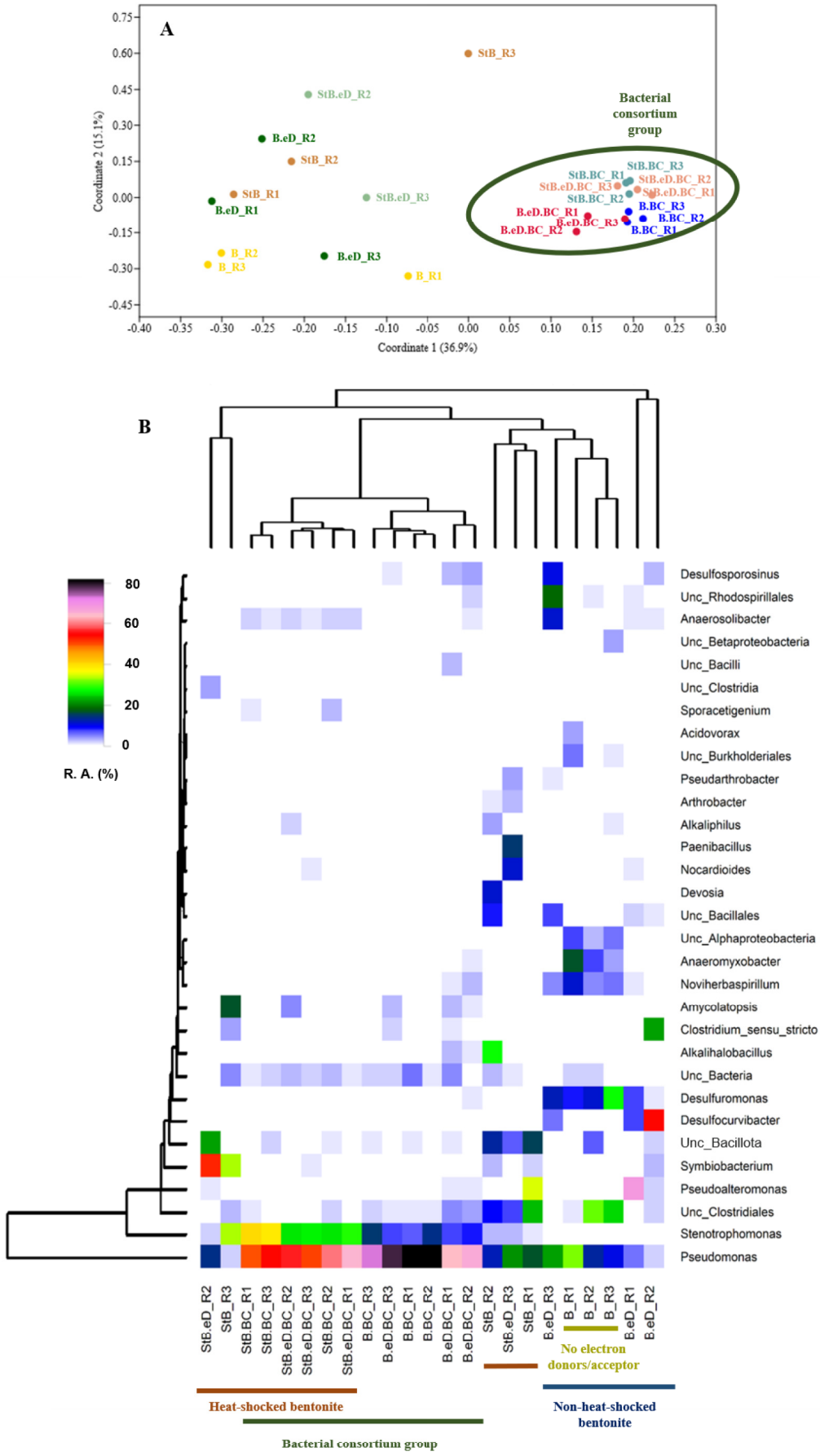
A
Coordinate 2 (15.1%)
Coordinate 1 (36.9%)
StB_R3
StB.eD_R2
B.eD_R2
StB_R2
StB_R1
B.eD_R1
StB.eD_R3
B_R2
B_R3
B.eD_R3
B_R1
Bacterial consortium group
StB.BC_R3
StB.BC_R1
StB.eD.BC_R2
StB.eD.BC_R3
StB.eD.BC_R1
StB.BC_R2
B.BC_R3
B.eD.BC_R1
B.BC_R2
B.eD.BC_R3
B.eD.BC_R2
B.BC_R1
B
R. A. (%)
Desulfosporosinus
Unc_Rhodospirillales
Anaerosolibacter
Unc_Betaproteobacteria
Unc_Bacilli
Unc_Clostridia
Sporacetigenium
Acidovorax
Unc_Burkholderiales
Pseudarthrobacter
Arthrobacter
Alkaliphilus
Paenibacillus
Nocardioides
Devosia
Unc_Bacillales
Unc_Alphaproteobacteria
Anaeromyxobacter
Noviherbaspirillum
Amycolatopsis
Clostridium_sensu_stricto
Alkalihalobacillus
Unc_Bacteria
Desulfuromonas
Desulfocurvibacter
Unc_Bacillota
Symbiobacterium
Pseudoalteromonas
Unc_Clostridiales
Stenotrophomonas
Pseudomonas
StE.eD_R2
StB_R3
StB.BC_R1
StB.BC_R3
StB.eD.BC_R2
StB.BC_R2
StB.eD.BC_R3
StB.BC_R3
B.eD.BC_R3
B.BC_R1
B.BC_R2
B.eD.BC_R1
B.eD.BC_R2
StB_R2
StB.eD_R3
StB_R1
B.eD_R3
B_R1
B_R2
B_R3
B.eD_R1
B.eD_R2
No electron donors/acceptor
Heat-shocked bentonite
Non-heat-shocked bentonite
Bacterial consortium group

Figure 4. **A:** Principal coordinate analysis (PCoA) plot showing the dissimilarity of bacterial communities at genus level from bentonite-slurry microcosms after 45 days of anaerobic incubation. **B**: Heatmap representing genus-level relative abundance and clustering based on Manhattan distance of the slurry-bentonite microcosms after 45 days of incubation. The 3.3% cut-off based on the maximums represents the 31 most abundant genera. The relative abundance of each genus is shows with different colors (the warmer the color, the greater relative abundance). Glossary: B: bentonite, StB: heat-shocked bentonite, eD: addition of electron donors and sulfate, BC: spiked with bacterial consortium

As observed in the chemical evolution data (**Figure 2**), samples spiked with bacterial consortium (BC) showed the highest rate of lactate consumption after 45 days of incubation, and the highest consumption (B.eD.BC) or production (StB.eD.BC) of acetate. *Pseudomonas* and *Stenotrophomonas* could be key contributors to the observed trend of lactate consumption and acetate production/consumption in samples amended with electron donors/acceptor (eD) (Essén et al., 2007; Eschbach et al., 2004; Ruiz-Fresneda et al., 2019; Sanchez-Castro et al., 2017). Moreover, in sample B.eD.BC, the presence of the sulfate-reducing bacterium *Desulfosporosinus* (**Supplementary Table S5** and **Figure 5**) was evidenced (2.62%). This bacterium is involved in the incomplete oxidation of substrates, such as lactate to acetate, and in the use of sulfate as a terminal electron acceptor (Spring and Rosenzweig, 2006). This fact could be linked to the sulfate consumption (≈ 50%) within this sample at the 45-day mark (**Figure 2C**). In contrast, sample StB.eD.BC did not show sulfate reduction **(Figure 2C**). This could be attributed to the absence of *Desulfosporosinus* in this treatment and the presence of the IRB and SRB *Anaerosolibacter* (1.83%; **Supplementary Table S4** and **Figure 4**). The dominance between sulfate reduction and iron reduction depends on pH, iron crystallinity, and their concentrations. In this experiment, with a neutral pH and a high sulfate concentration,

sulfate reduction is likely more favorable. Therefore, the presence of this bacterial genus may indicate that the redox conditions are not yet optimal for sulfate reduction to occur.

The addition of electron donors and sulfate in samples not spiked with bacterial consortium appears to enhance the prevalence of bacterial genera such as *Desulfocurvibacter* (obligately anaerobic SRB that incompletely oxidize organic substrates to acetate), *Pseudoalteromonas* (IRB under low content of oxygen), *Anaerosolibacter* (IRB and SRB), and *Desulfosporosinus* (anaerobic bacteria that reduce sulfate through the incomplete oxidation of lactate to acetate) (Spring et al., 2019; Cheng et al., 2019; Stackebrandt et al., 1997). These genera exhibit high diversity in sample B.eD (22.72%, 24.17%, 4.54%, and 4.54%, respectively), whereas they were not detected, or detected in a very low abundance, in sample B (< 0.2%) (**Supplementary Table S5** and **Figure 5**). Despite the presence of SRB in the B.eD treatment, no observable sulfate

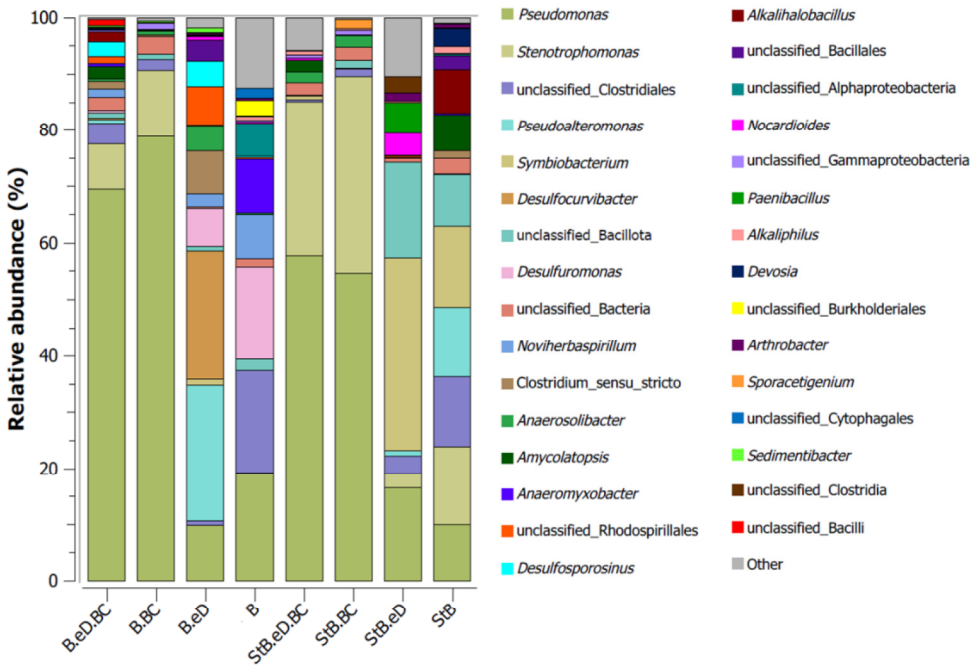

Figure 5. OUT relative abundance of bacterial communities from the bentonite slurry microcosms. Cutoff: 0.20% of relative abundance. Stacked bars show averages of biological replicates. Glossary: B: bentonite, StB: heat-shocked bentonite, eD: addition of electron donors and sulfate, BC: spiked with bacterial consortium.

consumption was detected (**Figure 2C**). This lack of consumption could be attributed to the limited time available for this process (45 days), as IRB such as *Pseudomonas* (9.80%), *Anaerosolibacter* (4.54%), and *Pseudoalteromonas* (24.17%) might be actively engaged in the fermentation of lactate to acetate and propionate as suggested by Park et al. (2024). The resulting acetate could be then used to promote the reduction of Fe(III) to Fe(II). This reduction process may continue until the redox conditions within the microcosms become favorable for sulfate reduction. Moreover, the most abundant genera in sample B were *Pseudomonas* (19.11%), unclassified Clostridiales (18.25%), *Desulfuromonas* (16.37%), *Anaeromyxobacter* (9.57%), and *Noviherbaspirillum* (7.77%) being less abundant in the B.eD treatment (**Supplementary Table S5** and **Figure 5**). *Desulfuromonas* has the capacity to couple the oxidation of acetate and lactate with the reduction of sulfate (Liesack and Finster 1994). The occurrence of *Pseudomonas*, *Anaeromyxobacter*, and *Noviherbaspirillum*, all facultative anaerobes, indicated their capability to use acetate and/or lactate as carbon sources (Shrestha et al., 2022; Sanford et al., 2002; Ishii et al., 2017). On the other hand, *Symbiobacterium* was the most abundant genus within heat-shocked samples without bacterial consortium (StB.eD: 34.11%, and StB: 14.39%). Bacterial species within this genus, including *S. turbinis* and *S. terraclitae*, are moderately anaerobic and thermophilic, with the characteristic of occasional endospore formation. Furthermore, these bacteria are capable of producing acetate as end product (Shiratori-Takano et al., 2014). The presence of this bacterial genus within the StB.eD.BC sample could suggest a contribution to the increase in acetate content observed in this treatment after 45 days of incubation (**Figure 2B**). Moreover, in the heat-shocked sample without a bacterial consortium (StB), *Stenotrophomonas* (13.98%), unclassified Clostridiales (12.39%), *Pseudoalteromonas* (12.36%), *Pseudomonas* (9.91%), unclassified Bacillota (9.12%), the facultatively anaerobic *Alkalihalobacillus*

374 (7.81%), and *Amycolatopsis* (6.44%), were the most prevalent bacterial genera following
375 *Symbiobacterium*.

376 In summary, the addition of the bacterial consortium had an impact on the shift of
377 indigenous bentonite microbial community. However, it is noteworthy that only
378 *Pseudomonas* and *Stenotrophomonas* managed to persist and prevail in the BC
379 microcosms after 45 days of incubation, whereas *Amycolatopsis* and *Bacillus* exhibited
380 lower abundances or fell below the detection threshold of the sequencing procedure.
381 Furthermore, the presence of specific bacterial genera was intricately linked to the
382 consumption of lactate, acetate and sulfate within the samples at 45 days of anaerobic
383 incubation. Given the complexity and heterogeneity of the bacterial diversity, it is
384 plausible that each bacterium may exhibit a distinct metabolic profile. Thus, the total
385 reaction computation observed in the **Figure 2** does not align stoichiometrically with a
386 simple system or an isolated bacterial strain study. Some bacteria (e.g.,
387 *Desulfosporosinus*) are able to partially oxidize lactate, associated with sulfate reduction,
388 leading to the production of acetate. This acetate, in turn, could serve as a carbon source
389 for other bacterial groups. Conversely, the addition of electron donors and sulfate appears
390 to stimulate the presence of IRB and SRB (e.g., *Desulfocurvibacter*, *Pseudoalteromonas,*
391 *Anaerosolibacter,* and *Desulfosporosinus*). These groups of bacteria are involved in the
392 corrosion of metal canisters within the DGR (Schütz et al., 2015; Bengtsson and Pedersen,
393 2017). However, the sulfate consumption was only detected at 45 days of incubation in
394 the sample B.eD.BC (≈ 50%). Hence, it is crucial to investigate the potential impact of
395 these bacterial groups on the corrosion of copper material and characterize the resulting
396 products.

3.3_ Characterization of the Cu canister surface in an early-incubation stage

In order to assess the influence of the microbial communities on the corrosion of the copper surface after 45-day incubation, the Cu-mCan were recovered from the studied microcosms. The metal surfaces were analyzed by microscopic and spectroscopic techniques (HRSEM, EDX, and XPS). Specifically, the analysis focused on Cu-mCan from microcosms with non-heat-shocked bentonite.

The Cu-mCan images of samples before (t. 0) and after 45 days and their HRSEM micrographs are shown in **Figure 6**. The bentonite adhered to the copper surface was not removed to avoid the consequent displacement of copper alteration-related products. Visually, the samples exhibited a different coloration after the incubation comparing with the blank (t. 0). The sample B.eD.BC presented a marked color transformation, shifting to dark gray-black hues, as well as some zones on Cu-mCan B.BC (**Figure 6_B,C)**. At microscopic level, the samples after the incubation exhibit a heterogenous topography (second column, **Figure 6**). The sample t. 0 displayed a uniform topography, revealing only the presence of Cu and C (attributable to the metallization process during the sample preparation). Furthermore, elemental EDX map of Iron (Fe), Carbon (C), Aluminum (Al), Sulfur (S), Silicon (Si), Oxygen (O), and Copper (Cu) distribution of the selected areas is shown (**Figure 6)**. The signal of Si (pink), Fe (yellow), and Al (cyan) were attributed to the presence of bentonite adhered on the Cu surface. The detection of O (red) was mainly associated with Si (Si_xO) linking with the presence of bentonite.

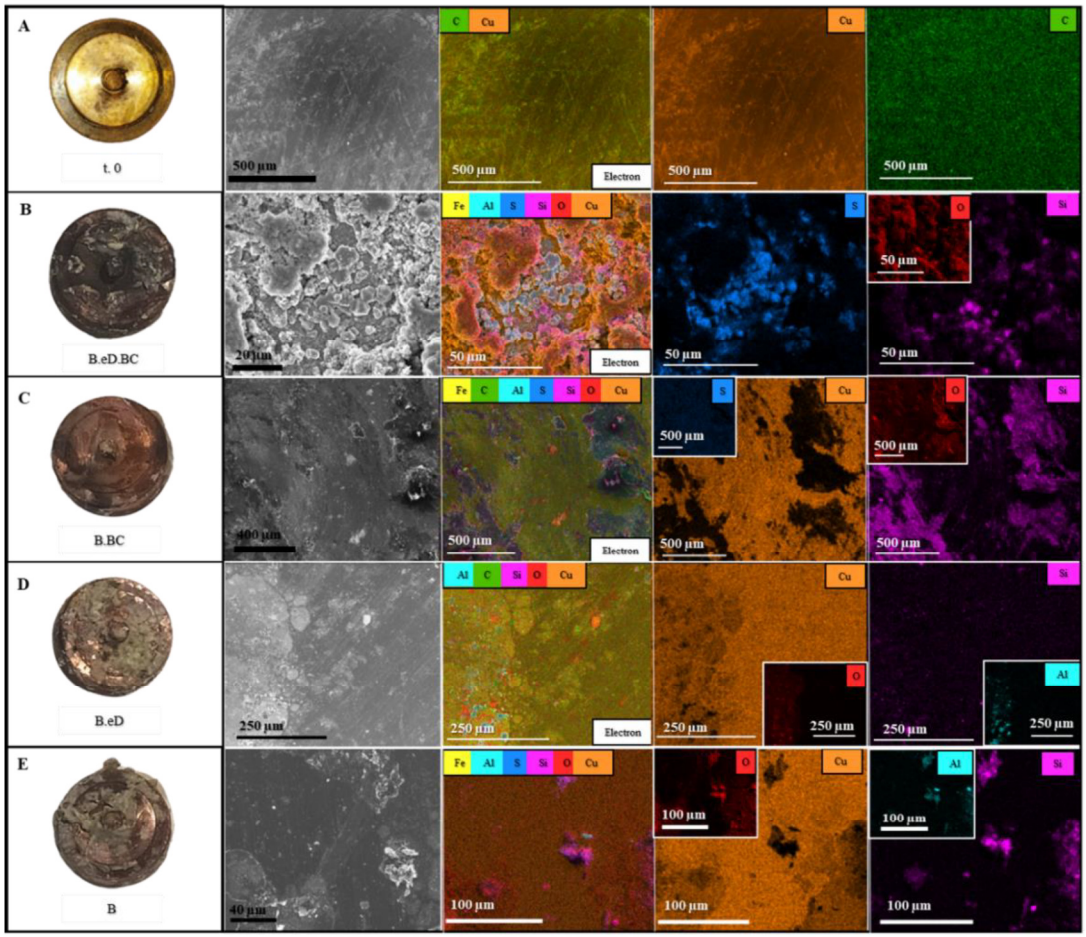

Figure 6. Visual (first column), electron images (second column), and EDX maps of the Cu-mCan surface before experimental set-up (A) and after 45-days anoxic incubation from microcosms B.eD.BC (B), B.BC (C), B.eD (D), and B (E). EDX show the distribution of Cu (orange), Fe (yellow), S (dark blue), Si (pink), Al (cyan), O (red), and C (green) in the studied area. Glossary: B: bentonite, StB: heat-shocked bentonite, eD: addition of electron donors and sulfate, BC: spiked with bacterial consortium.

417 Moreover, O was also detected, to a lesser extent, on the copper surface (Cu_xO). Sulfur
418 precipitates were only detected in the sample B.eD.BC, which may be related to Cu_xS
419 (copper corrosion compounds) (**Figure 6_B**) linking with the data of sulfate consumption
420 (≈ 50%, **Figure 2C**). Diffuse S accumulates distributed more dispersed manner were also
421 detected in sample B.BC (**Figure 6_C**). Furthermore, in sample B.eD, the presence of
422 oxygen seemed to be closely related to irregularities on the copper surface probably
423 related to the presence of copper oxides (Cu_xO).

424 In order to identify the nature of the corrosion products, XPS analysis was undertaken in
425 each Cu-mCan. Wide scans indicated the presence of Cu, C, O, Si, Na, Fe, Mg, and Al on

all sample surfaces. Except for Cu, these elements were attributed to bentonite adhered to the Cu-mCan's surfaces. High-resolution scans of the Cu 2p region exhibited elemental copper peaks (sharp peaks at approximately 933 eV and 953 eV, corresponding to Cu $2p_{1/2}$ and Cu $2p_{3/2}$), alongside the likely presence of CuO (peaks around 943.49 eV and 962.89 eV) (Wagner et al., 1979), on all samples (**Figure 7**). Further evidence for the existence of CuO included the separation of ≈ 20 eV between Cu $2p_{1/2}$ and Cu $2p_{3/2}$ (Wagner et al., 1979). It should be noted that no CuO was detected on the surface of the Cu-mCan prior to microcosms set up (time 0) as shown in the high-resolution spectra of the Cu 2p (**Figure 7**).

The main signal of MIC under anaerobic corrosion on copper materials are Cu_xS mediated by the activity of SRB (Hall et al., 2021). Previous studies indicate that peaks for CuS are typically observed around 932.2 eV in high-resolution Cu 2p scans (Krylova & Andrulevičius, 2009). In order to delve deeper into the overshadow of this peak by the Cu $2p_{3/2}$ peak, high-resolution scans were conducted in the S 2p region, spanning from 143 eV to 180 eV. This revealed the presence of sulfur on samples B.BC, B.eD.BC, and B.eD (**Figure 7**). In samples B.BC and B.eD.BC, peaks related to the presence of Cu_2S (around 163 eV) were seen. This is a known corrosion product produced as a result of HS^- excretion from SRB activity (Martinez-Moreno et al., 2023; Yu et al., 1990). Moreover, the peak at 161.4 eV was assigned to CuS (Kutty, 1991). The peak around 154

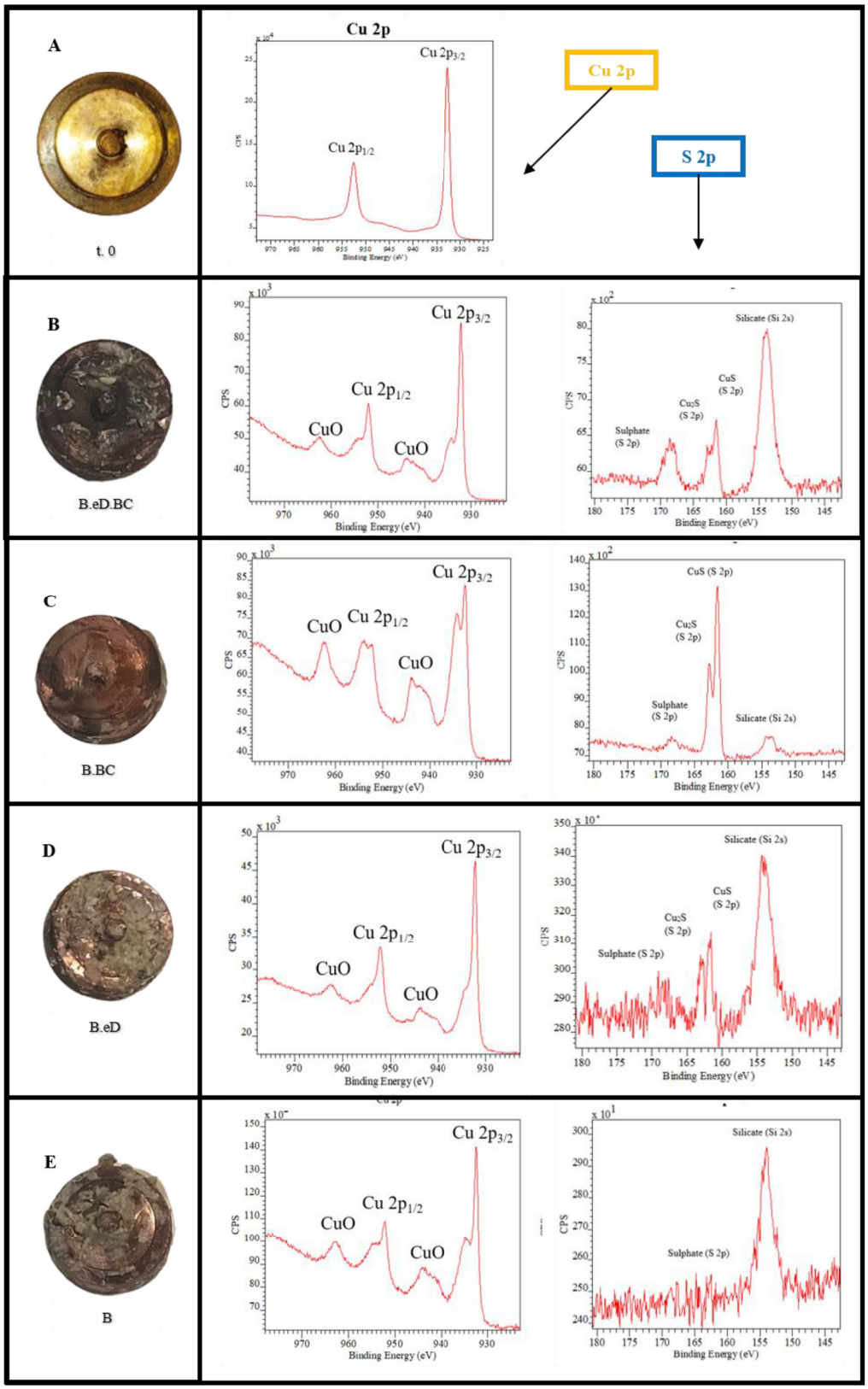

Figure 7. High-resolution XPS spectra of the Cu 2p (977 eV – 922 eV) and S 2p (180 eV – 143 eV) regions of the Cu-mCan surface before experimental set-up (A) and after 45-days anoxic incubation from microcosms B.eD.BC (B), B.BC (C), B.eD (D), and B (E). Glossary: B: bentonite, StB: heat-shocked bentonite, eD: addition of electron donors and sulfate, BC: spiked with bacterial consortium.

445 eV, presented in all the Cu-mCan after 45-days incubation, was attributed to Si 2s in the

446 form of SiO_2 (silicate) belonging to the presence of the bentonite adhered on the copper
447 surface (Clarke & Rizkalla, 1976).

448 Given that copper oxides (CuO) were identified on all Cu-mCan samples after 45 days of
449 incubation, notably absent at t. 0, it can be inferred that the presence of oxygen, evidenced
450 by CuO on the copper surface, occurred abiotically. The formation of the CuO species
451 could be related to the oxygen molecules trapped in the bentonite or driven by the
452 reduction of H_2O from the EW (Burzan et al., 2022; Huttunen-Saarivirta et al., 2016).
453 Conversely, the identification of Cu_2S in the samples resulted from microbial influence.
454 This observation was particularly pronounced on the surface of Cu-mCan from the
455 treatment with electron donors/acceptor and the bacterial consortium (B.eD.BC),
456 followed by the treatment only spiked with the bacterial consortium (B.BC). Additionally,
457 a lesser extent of Cu_2S detection was detected in the treatment supplemented only with
458 electron donors/acceptor (B.eD). In contrast, Cu_2S was not detected in treatment B
459 (untreated bentonite) (**Figure 6** and **Figure 7**). Moreover, microscopic examination
460 revealed the presence of precipitates of Cu_2S compounds exclusively in Cu-mCan from
461 the treatment B.eD.BC (**Figure 6**), aligning with the heightened presence of SRB within
462 this treatment (**Figure 5** and **Supplementary Table S5**).

463 The production of sulfide through the reduction of sulfate is kinetically hindered under
464 standard abiotic conditions of temperature and pressure (Cross et al., 2004). Thus, the
465 presence of sulfide is likely to be attributed to the activity of SRB (Bengtsson and
466 Pedersen, 2017). Under anoxic conditions SRB can oxidize lactate as electron donor (**Eq.**
467 **1)** coupled to sulfate reduction as terminal electron acceptor through the dissimilatory
468 sulfate reduction (**Eq. 2**) (Dou et al., 2020). The production of the sulfide in the
469 microcosms was also inferred by the characteristic rotten egg smell in the microcosms
470 (He et al., 2011). Interestingly, Salehi Alaei et al. (2023) observed the conversion of

copper oxides (Cu_2O) to Cu_2S by a chemical substitution reaction between sulfide and the oxide (**Eq. 3**). Additionally, Dou et al. (2020) proposed that the resulting metabolite HS^-, from H_2S secreted by SRB, can diffuse to the surface and react with copper to form Cu_2S (**Eq. 4**).

Eq. 1: $CH_3CHOHCOO^- + H_2O \rightarrow CH_3COO^- + CO_2 + 4H^+ + 4e^-$

Eq. 2: $SO_4^{2-} + 9H^+ + 8e^- \rightarrow HS^- + 4H_2O$

Eq. 3: $Cu_2O + SH^- \rightarrow Cu_2S + OH^-$

Eq. 4: $2Cu + HS^- + H^+ \rightarrow Cu_2S + H_2$

Chen et al. (2014) demonstrated that under anaerobic conditions, SRB can form a Cu_2S film as the primary corrosion product. The production of extracellular polymeric substances (EPS) from the SRB biofilm, and subsequently the Cu_2S film, mitigates the toxicity of copper toward SRB. In experiments with copper and different SRB strains, Kurmakova et al. (2019) found that these bacteria were accountable for Cu_2S corrosion products, with *Desulfovibrio* sp. M.4.1 showing the highest corrosive impact on the metal surface. The corrosion of high-purity copper in the presence of SRB in groundwater borehole or MX-80 clay has been demonstrated in other studies, where the presence of Cu_2S precipitates was detected (Johansson et al., 2017; Masurat et al., 2010). The addition of acetate, lactate, and sulfate to Spanish bentonite has been demonstrated to enhance bacterial activity, leading to the development of small corrosion compounds on copper discs within compacted bentonite blocks in the absence of water flow renewal after one year of anoxic incubation (Martinez-Moreno et al., 2023). The presence of an aqueous phase (EW) in this study accelerated this process, with corrosion compound formation observed in an early-stage of incubation (45 days).

4_ Study overview and conclusions

The surrounded environment of future DGR is considered hostile to organisms' survival (e.g., high temperature due to heat generated by the decay process of the radionuclides, low water activity close to the canisters, high compaction of the bentonite, etc.). All these possible scenarios should be considered when assessing the release of radionuclides and their migration to the biosphere over periods of time spanning hundreds of thousands to millions of years. Here, ideal conditions for microorganism's survival and activity, bentonite slurry microcosms amended with electron donors/acceptor, were simulated. Although the DGR is designed to hinder the diffusion of pore water into the canisters, the flow of nutrients within the groundwater is not discarded. Consequently, examining laboratory-scale models is crucial in generating new insights on the biogeochemical processes under different scenarios.

This study describes the geochemical evolution of the bentonite slurry microcosms over a year-long anaerobic incubation at 30 ºC, and in an early-stage (45 days) microbial-community characterization and its influence in the corrosion of copper material. A trend towards pH stabilization was observed, which could be linked to the biotic processes (generation of biogenic gases like H_2, CH_4, or CO_2) and the buffering properties of the bentonite. The consumption of lactate was the most pronounced, coupled with the formation of acetate and hydrogen sulfide in the microcosms. These finding were supported by the observation of fissures in the bentonite and the smell of rotten eggs after sampling. Moreover, the produced sulfide can react with the iron within the bentonite, causing their color shift to grayish-blackish hues. It is important to highlight that the ideal conditions consisted in amended bacterial consortium and added electron donors/acceptor, significantly accelerated biogeochemical processes, whereas the tyndallization of the bentonite had a retarding effect.

519 The amended BPAS consortium was found to reduce the microbial diversity in the
520 microcosms at the early stage (45 days), with *Pseudomonas* and *Stenotrophomonas*
521 emerging as the predominant bacteria. Conversely, microcosms lacking BPAS consortium
522 and amended with electron donors/acceptor or with heat-shocked bentonite exhibited
523 higher microbial diversity and heterogeneity. However, the addition of electron
524 donors/acceptor helped with the stimulation of certain bacterial groups such as SRB,
525 playing an important role in the formation of corrosion products on the copper surface.

526 Under anaerobic conditions, SRB are capable of oxidizing electron donors (e.g., lactate)
527 coupled to sulfate reduction through dissimilatory sulfate reduction pathway. The
528 produced sulfide could mediate the conversion of copper oxides (possibly formed by
529 trapped oxygen molecules on the bentonite or driven by the reduction of H_2O from the
530 EW) to copper sulfide (Cu_2S) by a chemical substitution reaction between sulfides and
531 oxides, or by the diffusion of and reaction of HS^- to copper.

532 Overall, microorganisms will play an important role in the geochemical evolution within
533 the DGR and the stability of the different barriers could be compromised, emphasizing
534 the impact of the SRB on the corrosion of the metal canisters, the gas generation, and the
535 interaction with components of the bentonite.

536 **Funding**

537 The present work was supported by the grant RTI2018–101548-B-I00 "ERDF A way of
538 making Europe" to MLM from the "Ministerio de Ciencia, Innovación y Universidades"
539 (Spanish Government). The project leading to this application has received funding from
540 the European Union's Horizon 2020 research and innovation program under grant
541 agreement No 847593 to MLM. ADM acknowledges funding from the UK Engineering

and Physical Sciences Research Council (EPSRC) DTP scholarship (project reference: 2748843).

Acknowledgements

The authors acknowledge the assistance of Dr. F. Javier Huertas (IACT, Spain) for his guidance and help in collecting the bentonite from the El Cortijo de Archidona site (Almería). Rahul N. Doulatram Gamgaram and Maria del Carmen Contreras Morales (Institute of Water Research, University of Granada) for HPIC measurements. Moreover, Daniel García-Muñoz Bautista-Cerro and Alicia González Segura (Centro de Instrumentación Cientifica, University of Granada, Spain) for the sample preparation and microscopy assistance, respectively.

References

Bagnoud, A., De Bruijn, I., Andersson, A. F., Diomidis, N., Leupin, O. X., Schwyn, B., & Bernier-Latmani, R. 2016. A minimalistic microbial food web in an excavated deep subsurface clay rock. FEMS Microb. Ecol., 92(1), fiv138. https://doi.org/10.1093/femsec/fiv138

Batandjieva, B., Delcheva, T., Duhovnik, B. 2009. Classification of radioactive waste: safety guide: IAEA General Safety Guide GSG-1. Vienna. International Atomic Energy Agency.

Bengtsson, A., Pedersen, K. 2017. Microbial sulphide-producing activity in water saturated Wyoming MX-80, Asha and Calcigel bentonites at wet densities from 1500 to 2000 kg m^{-3}. Appl. Clay Sci. 137, 203-212. https://doi.org/10.1016/j.clay.2016.12.024

Bohorquez, L.C., Delgado-Serrano, L., López, G., Osorio-Forero, C., Klepac-Ceraj, V., Kolter, R., Junca, H., Baena, S., Zambrano, M.M., 2012. In-depth Characterization via Complementing Culture-Independent Approaches of the Microbial Community in an Acidic Hot Spring of the Colombian Andes. Micro Ecol. 63, 103–115. https://doi.org/10.1007/s00248-011-9943-3

Burzan, N., Murad Lima, R., Frutschi, M., Janowczyk, A., Reddy, B., Rance, A., ... & Bernier-Latmani, R. 2022. Growth and persistence of an aerobic microbial Community in Wyoming Bentonite MX-80

despite anoxic in situ conditions. Frontiers in Microbiology, 13, 858324. https://doi.org/10.3389/fmicb.2022.858324

Cheng, S., Li, N., Jiang, L., Li, Y., Xu, B., & Zhou, W. 2019. Biodegradation of metal complex Naphthol Green B and formation of iron–sulfur nanoparticles by marine bacterium *Pseudoalteromonas* sp CF10-13. Bioresour. Technol., 273, 49-55. https://doi.org/10.1016/j.biortech.2018.10.082

Chen, S., Wang, P., Zhang, D. 2014. Corrosion behavior of copper under biofilm of sulfate-reducing bacteria. Corros. Sci. 87, 407 – 415. http://dx.doi.org/10.1016/j.corsci.2014.07.001

Clarke, T. A., & Rizkalla, E. N. 1976. X-ray photoelectron spectroscopy of some silicates. Chem. Phys. Lett., 37(3), 523-526. https://doi.org/10.1016/0009-2614(76)85029-4

Cross, M.M., Manning, D.A., Bottrell, S.H., Worden, R.H. 2004. Thermochemical sulphate reduction (TSR): experimental determination of reaction kinetics and implications of the observed reaction rates for petroleum reservoirs. Org. Geochem. 35, 393–404. https://doi.org/10.1016/j.orggeochem.2004.01.005

Dou, W., Pu, Y., Han, X., Song, Y., Chen, S., Gu, T. 2020. Corrosion of Cu by a sulfate reducing bacterium in anaerobic vials with different headspace volumes. Bioelectrochemistry, 133, 107478. https://doi.org/10.1016/j.bioelechem.2020.107478

Eschbach, M., Schreiber, K., Trunk, K., Buer, J., Jahn, D., & Schobert, M. 2004. Long-term anaerobic survival of the opportunistic pathogen *Pseudomonas aeruginosa* via pyruvate fermentation. J. Bacteriol., 186(14), 4596-4604. https://doi.org/10.1128/jb.186.14.4596-4604.2004

Essén, S. A., Johnsson, A., Bylund, D., Pedersen, K., & Lundström, U. S. 2007. Siderophore production by *Pseudomonas stutzeri* under aerobic and anaerobic conditions. Appl. Environ. Microbiol.73(18), 5857-5864. https://doi.org/10.1128/AEM.00072-07

Fairley, N. CasaXPS, 2.3.22 ed.; Casa Software Ltd.: 2019.

Fernández, A.M. (2004). Caracterización y modelización del agua intersticial de materiales arcillosos: Estudio de la bentonita de Cortijo de Archidona. Editorial Ciemat. ISBN84-7834-479-9, 505 pp.

Freikowski, D., Winter, J., & Gallert, C. (2010). Hydrogen formation by an arsenate-reducing Pseudomonas putida, isolated from arsenic-contaminated groundwater in West Bengal, India. Appl. Microbiol. Biotechnol., 88, 1363-1371. https://doi.org/10.1007/s1201000988520

García-Romero, E., María Manchado, E., Suárez, M., and García-Rivas, J. 2019. Spanish bentonites: a review and new data on their geology, mineralogy, and crystal chemistry. Fortschr. Mineral. 9:696. https://doi.org/10.3390/min9110696

Guo, G., & Fall, M. 2021. Advances in modelling of hydro-mechanical processes in gas migration within saturated bentonite: A state-of-art review. Eng. Geol., 287, 106123. https://doi.org/10.1016/j.enggeo.2021.106123

Hall, D.S., Behazin, M., Binns, W.J., and Keech, P.G. 2021. An evaluation of corrosion processes affecting copper-coated nuclear waste containers in a deep geological repository. Prog. Mater. Sci. 118, 100766. https://doi.org/10.1016/j.pmatsci.2020.100766

Hammer, O. 2001. PAST: paleontological statistics software package for education and data analysis. Palaeontol. Electron. *http://palaeo-electronicaorg*

He, R., Xia, F. F., Wang, J., Pan, C. L., & Fang, C. R. 2011. Characterization of adsorption removal of hydrogen sulfide by waste biocover soil, an alternative landfill cover. J. Hazard. Mater., 186(1), 773-778. https://doi.org/10.1016/j.jhazmat.2010.11.062

Hippe, H., & Stackebrandt, E. 2015. *Desulfosporosinus*. Bergey's Manual of Systematics of Archaea and Bacteria, 1-10. https://doi.org/10.1002/9781118960608.gbm00660

Hong, H., Kim, S. J., Min, U. G., Lee, Y. J., Kim, S. G., Roh, S. W., ... & Rhee, S. K. 2015. *Anaerosolibacter carboniphilus* gen. nov., sp. nov., a strictly anaerobic iron-reducing bacterium isolated from coal-contaminated soil. Int. J. Syst. Evol. Microbiol., 65(Pt_5), 1480-1485. https://doi.org/10.1099/ijs.0.000124

Huertas, F., Fariña, P., Farias, J., García-Siñeriz, J.L., Villar, M.V., Fernández, A.M., Martin, P.L., Elorza, F.J., Gens, A., Sánchez, M., Lloret, A., Samper, J., Martínez, M. Á. 2021. Full-scale Engineered Barriers Experiment. Updated Final Report 1994-2004.

Huttunen-Saarivirta, E., Rajala, P., & Carpén, L. 2016. Corrosion behaviour of copper under biotic and abiotic conditions in anoxic ground water: Electrochemical study. Electrochim. Acta, 203, 350-365. https://doi.org/10.1016/j.electacta.2016.01.098

Ishii, S., Ashida, N., Ohno, H., Segawa, T., Yabe, S., Otsuka, S., ... & Senoo, K. 2017. *Noviherbaspirillum denitrificans* sp. nov., a denitrifying bacterium isolated from rice paddy soil and *Noviherbaspirillum autotrophicum* sp. nov., a denitrifying, facultatively autotrophic bacterium isolated from rice paddy

soil and proposal to reclassify *Herbaspirillum massiliense* as *Noviherbaspirillum massiliense* comb. nov. Int. J. Syst. Evol. Microbiol., 67(6), 1841-1848. https://doi.org/10.1099/ijsem.0.001875

Johansson, A.J., Lilja, C., Sjögren, L., Gordon, A., Hallbeck, L., Johansson, L. 2017. Insights from post-test examination of three packages from the MiniCan test series of coppercast iron canisters for geological disposal of spent nuclear fuel: impact of the presence and density of bentonite clay. Corros. Eng. Sci. Technol. 52, 54-60. https://doi.org/10.1080/1478422X.2017.1296224

Keech, P. G., Vo, P., Ramamurthy, S., Chen, J., Jacklin, R., Shoesmith, D. W. 2014. Design and development of copper coatings for long term storage of used nuclear fuel. Corros. Eng. Sci. Technol., 49(6), 425-430. https://doi.org/10.1179/1743278214Y.0000000206

Krylova, V., Andrulevičius, M. 2009. Optical, XPS and XRD studies of semiconducting copper sulfide layers on a polyamide film. Int. J. Photoenergy. https://doi.org/10.1155/2009/304308

Kurmakova, I., Kupchyk, O., Bondar, O., Demchenko, N., & Vorobyova, V. 2019. Corrosion of copper in a medium of bacteria sulfate reduction proceeding. J. Chem. Technol. Metall., 54, 2, 2019, 416-422.

Kutty, T. R. N. 1991. A controlled copper-coating method for the preparation of ZnS: Mn DC electroluminescent powder phosphors. Mater. Res. Bull., 26(5), 399-406. https://doi.org/10.1016/0025-5408(91)90054-P

Liesack, W., & Finster, K. 1994. Phylogenetic analysis of five strains of gram-negative, obligately anaerobic, sulfur-reducing bacteria and description of *Desulfuromusa* gen. nov., including *Desulfuromusa kysingii* sp. nov., *Desulfuromusa bakii* sp. nov., and *Desulfuromusa succinoxidans* sp. nov. Int. J. Syst. Evol. Microbiol., 44(4), 753-758. https://doi.org/10.1099/00207713-44-4-753

Liu, D., Dong, H., Bishop, M.E., Zhang, J., Wang, H., Xie, S., Wang, S., Huang, L., Eberl, D.D. 2012. Microbial reduction of structural iron in interstratified illite-smectite minerals by a sulfate-reducing bacterium. Geobiology, 10, 150-162. https://doi.org/10.1111/j.1472-4669.2011.00307.x

Martinez-Moreno, M.F., Povedano-Priego, C., Morales-Hidalgo, M., Mumford, A.D., Ojeda, J.J., Jroundi, F., Merroun, M. L. 2023. Impact of compacted bentonite microbial community on the clay mineralogy and copper canister corrosion: a multidiskiplinary approach in view of a safe Deep Geological Repository of nuclear wastes. J. Hazard. Mater. 131940. https://doi.org/10.1016/j.jhazmat.2023.131940

Masurat, P., Eriksson, S., Pedersen, K. 2010. Microbial sulphide production in compacted Wyoming bentonite MX-80 under in situ conditions relevant to a repository for high-level radioactive waste. Appl. Clay Sci. 47, 58-64. https://doi.org/10.1016/j.clay.2009.01.004

Matschiavelli, N., Kluge, S., Podlech, C., Standhaft, D., Grathoff, G., Ikeda-Ohno, A., ... & Cherkouk, A. 2019. The year-long development of microorganisms in uncompacted bavarian bentonite slurries at 30 and 60 ºC. Environ. Sci. Technol. 2019, 53, 10514−10524. https://doi.org/10.1021/acs.est.9b02670

Meleshyn, A. 2011. Microbial processes relevant for long-term performance of radioactive waste repositories in clays. GRS-291. ISBN 978-3-939355-67-0. Available from: https://www.grs.de/sites/default/files/pdf/GRS-291.pdf

Miettinen, H., Bomberg, M., Bes, R., Tiljander, M., & Vikman, M. 2022. Transformation of inherent microorganisms in Wyoming-type bentonite and their effects on structural iron. Appl. Clay Sci., 221, 106465. https://doi.org/10.1016/j.clay.2022.106465

Oh, Y. S., Park, A. R., Lee, J. K., Lim, C. S., Yoo, J. S., & Roh, D. H. (2011). *Pseudoalteromonas donghaensis* sp. nov., isolated from seawater. Int J Syst Evol Microbiol, 61(2), 351-355. https://doi.org/10.1099/ijs.0.022541-0

Ojovan, M.I.; Steinmetz, H.J. 2022. Approaches to Disposal of Nuclear Waste. Energies, 15, 7804. https://doi.org/10.3390/en15207804

Park, S. Y., Zhang, Y., O'Loughlin, E. J., Jo, H. Y., Kwon, J. S., & Kwon, M. J. 2024. Temperature-dependent microbial reactions by indigenous microbes in bentonite under Fe (III)-and sulfate-reducing conditions. J. Hazard. Mater., 465, 133318. https://doi.org/10.1016/j.jhazmat.2023.133318

Payer, J. H., Finsterle, S., Apps, J.A., Muller, R.A. 2019. Corrosion performance of engineered barrier system in deep horizontal drillholes. Energies. 12, 1491. https://doi.org/10.3390/en12081491

Pentráková, L., Su, K., Pentrák, M., Stucki, J.W. 2013. A review of microbial redox interactions with structural Fe in clay minerals. Clay Miner. 48, 543-560. https://doi.org/10.1180/claymin.2013.048.3.10

Povedano-Priego, C., Jroundi, F., Solari, P. L., Guerra-Tschuschke, I., del Mar Abad-Ortega, M., Link, A., ... & Merroun, M. L. 2023. Unlocking the bentonite microbial diversity and its implications in selenium bioreduction and biotransformation: Advances in deep geological repositories. J. Hazard. Mater., 445, 130557. https://doi.org/10.1016/j.jhazmat.2022.130557

683 Povedano-Priego, C., Jroundi, F., Lopez-Fernandez, M., Shrestha, R., Spanek, R., Martín-Sánchez, I.,
684 Villar, M.V., ˇSevců, A., Dopson, M. Merroun, M.L. 2021. Deciphering indigenous bacteria in
685 compacted bentonite through a novel and efficient DNA extraction method: Insights into
686 biogeochemical processes within the Deep Geological Disposal of nuclear waste concept. J. Hazard.
687 Mater. 408, 124600. https://doi.org/10.1016/j.jhazmat.2020.124600
688 Povedano-Priego, C., Jroundi, F., Lopez-Fernandez, M., Sánchez-Castro, I., Martin-Sánchez, I., Huertas,
689 F.J., Merroun, M.L. 2019. Shifts in bentonite bacterial community and mineralogy in response to
690 uranium and glycerol-2-phosphate exposure. Sci. Total Environ. 692, 219-232.
691 https://doi.org/10.1016/j.scitotenv.2019.07.228
692 Qin, Q. L., Li, Y., Zhang, Y. J., Zhou, Z. M., Zhang, W. X., Chen, X. L., ... & Zhang, Y. Z. 2011. Comparative
693 genomics reveals a deep-sea sediment-adapted life style of *Pseudoalteromonas* sp. SM9913. ISME
694 J 5, 274–284. https://doi.org/10.1038/ismej.2010.103
695 R Core Team. 2022. R: A language and environment for statistical computing. R Foundation for Statistical
696 Computing, Vienna, Austria. URL https://www.Rproject.org/
697 Robertson, C.E., Harris, J.K., Wagner, B.D., Granger, D., Browne, K., Tatem, B., Feazel, L.M., Park, K.,
698 Pace, N.R., Frank, D.N. 2013. Explicet: graphical user interface software for metadata-driven
699 management, analysis and visualization of microbiome data. Bioinformatics, 29, 3100-3101.
700 https://doi.org/10.1093/bioinformatics/btt526
701 Rozalén, M., Brady, P. V., & Huertas, F. J. 2009. Surface chemistry of K-montmorillonite: Ionic strength,
702 temperature dependence and dissolution kinetics. J. Colloid Interface Sci., 333(2), 474-484.
703 https://doi.org/10.1016/j.jcis.2009.01.059
704 Ruiz-Fresneda, M. A., Martinez-Moreno, M. F., Povedano-Priego, C., Morales-Hidalgo, M., Jroundi, F., &
705 Merroun, M. L. 2023. Impact of microbial processes on the safety of deep geological repositories
706 for radioactive waste. Front. Microbiol., 14, 1134078. https://doi.org/10.3389/fmicb.2023.1134078
707 Ruiz-Fresneda, M. A., Gomez-Bolivar, J., Delgado-Martin, J., Abad-Ortega, M. D. M., Guerra-Tschuschke,
708 I., & Merroun, M. L. 2019. The bioreduction of selenite under anaerobic and alkaline conditions
709 analogous to those expected for a deep geological repository system. Molecules, 24(21), 3868.
710 https://doi.org/10.3390/molecules24213868

711 Salehi Alaei, E., Guo, M., Chen, J., Behazin, M., Bergendal, E., Lilja, C., ... & Noël, J. J. 2023. The
712 transition from used fuel container corrosion under oxic conditions to corrosion in an anoxic
713 environment. Mater. Corros., 74(11-12), 1690-1706. https://doi.org/10.1002/maco.202313757
714 Sanchez-Castro, I., Ruiz-Fresneda, M. A., Bakkali, M., Kämpfer, P., Glaeser, S. P., Busse, H. J., ... &
715 Merroun, M. L. 2017. Stenotrophomonas bentonitica sp. nov., isolated from bentonite formations.
716 Int. J. Syst. Evol. Microbiol., 67(8), 2779. https://doi.org/10.1099%2Fijsem.0.002016
717 Sanford, R. A., Cole, J. R., & Tiedje, J. M. 2002. Characterization and description of *Anaeromyxobacter*
718 *dehalogenans* gen. nov., sp. nov., an aryl-halorespiring facultative anaerobic myxobacterium. Appl.
719 Environ. Microbiol., 68(2), 893-900. https://doi.org/10.1128/AEM.68.2.893-900.2002
720 Schütz, M. K., Schlegel, M. L., Libert, M., & Bildstein, O. 2015. Impact of iron-reducing bacteria on the
721 corrosion rate of carbon steel under simulated geological disposal conditions. Environ. Sci. Technol.,
722 49(12), 7483-7490. https://doi.org/10.1021/acs.est.5b00693
723 Shelobolina, E.S., VanPraagh, C.G., Lovley, D.R. 2003. Use of ferric and ferrous iron containing minerals
724 for respiration by Desulfitobacterium frappieri. Geomicrobiol. J. 20, 143-156.
725 https://doi.org/10.1080/01490450303884
726 Shiratori-Takano, H., Akita, K., Yamada, K., Itoh, T., Sugihara, T., Beppu, T., & Ueda, K. 2014. Description
727 of *Symbiobacterium ostreiconchae* sp. nov., *Symbiobacterium turbinis* sp. nov. and
728 *Symbiobacterium terraclitae* sp. nov., isolated from shellfish, emended description of the genus
729 *Symbiobacterium* and proposal of *Symbiobacteriaceae* fam. nov. Int. J. Syst. Evol. Microbiol.,
730 64(Pt_10), 3375-3383. https://doi.org/10.1099/ijs.0.063750-0
731 Shrestha, R., Cerna, K., Spanek, R., Bartak, D., Cernousek, T., & Sevcu, A. 2022. The effect of low-pH
732 concrete on microbial community development in bentonite suspensions as a model for microbial
733 activity prediction in future nuclear waste repository. Sci. Total Environ., 808, 151861.
734 https://doi.org/10.1016/j.scitotenv.2021.151861
735 Spring, S., Sorokin, D. Y., Verbarg, S., Rohde, M., Woyke, T., & Kyrpides, N. C. 2019. Sulfate-reducing
736 bacteria that produce exopolymers thrive in the calcifying zone of a hypersaline cyanobacterial mat.
737 Front. Microbiol., 10, 862. https://doi.org/10.3389/fmicb.2019.00862
738 Spring, S. & Rosenzweig, F. 2006. The genera *Desulfitobacterium* and *Desulfosporosinus*: taxonomy. The
739 prokaryotes, 4, 771-786. DOI: 10.1007/0-387-30744-3_24.

740 Stackebrandt, E., Sproer, C., Rainey, F. A., Burghardt, J., Päuker, O., & Hippe, H. 1997. Phylogenetic
741 analysis of the genus *Desulfotomaculum*: evidence for the misclassification of *Desulfotomaculum*
742 *guttoideum* and description of *Desulfotomaculum orientis* as *Desulfosporosinus orientis* gen. nov.,
743 comb. nov. Int. J. Syst. Evol. Microbiol., 47(4), 1134-1139. https://doi.org/10.1099/00207713-47-4-
744 1134
745 Villar, M.V., Fernández-Soler, J.M., Delgado Huertas, A., Reyes, E., Linares, J., Jiménez de Cisneros, C.,
746 Linares, J., Reyes, E., Delgado, A., Fernandez-Soler, J.M., Astudillo, J. 2006. The study of Spanish
747 clays for their use as sealing materials in nuclear waste repositories: 20 years of progress. J. Iber.
748 Geol. 32, 15-36.
749 Wagner, C.D., Riggs, W.M., Davis, L.E., Moulder, J.F., Muilenberg, G.E. 1979. Handbook of x-ray
750 photoelectron spectroscopy: a reference book of standard data for use in x-ray photoelectron
751 spectroscopy. Perkin-Elmer Corporation: Eden Prairie, MN.
752 WNA. World Nuclear Association. 2021. Storage and disposal of radioactive waste. https://www.world-
753 nuclear.org/
754 Yu, X. R., Liu, F., Wang, Z. Y., & Chen, Y. 1990. Auger parameters for sulfur-containing compounds using
755 a mixed aluminum-silver excitation source. J. Electron Spectrosc. Relat. Phenom., 50(2), 159-166.
756 https://doi.org/10.1016/0368-2048(90)87059-W